



DESIGNING NOVEL NANOMATERIALS FOR LI-ION BATTERIES: A PHYSICO-CHEMICAL STUDY THROUGH HYDROGEN-POWERED HORIZONS

 **Fateme Mollaamin**^{1*},  **Majid Monajjemi**²

¹Department of Biomedical Engineering, Faculty of Engineering and Architecture, Kastamonu University, Kastamonu, Turkiye

²Department of Chemical Engineering, Central Tehran Branch, Islamic Azad University, Tehran, Iran

Abstract. This research work intends to represent a comprehensive investigation on hydrogen grabbing by $\text{Si}_5\text{O}_{10}\text{-Ge}_5\text{O}_{10}$ was carried out including using density functional theory (DFT) computations. The data represents that if silicon elements are replaced by germanium, the H-grabbing energy will be ameliorated. Electromagnetic and thermodynamic properties of $\text{Si}_5\text{O}_{10}\text{-Ge}_5\text{O}_{10}$, $\text{Li}_2[\text{Si}_5\text{O}_{10}\text{-Ge}_5\text{O}_{10}]$ and nanoclusters have been evaluated. The hypothesis of the hydrogen adsorption phenomenon was confirmed by density distributions of charge density differences (CDD), total density of states (TDOS) and localized orbital locator (LOL) for hydrated nanoclusters of $\text{H}_2[\text{Si}_5\text{O}_{10}\text{-Ge}_5\text{O}_{10}]$ and $\text{Li}_2\text{H}_4[\text{Si}_5\text{O}_{10}\text{-Ge}_5\text{O}_{10}]$. The fluctuation in charge density values demonstrates that the electronic densities were mainly located in the boundary of adsorbate/adsorbent atoms during the adsorption status. Therefore, by combination of Si_5O_{10} and Ge_5O_{10} , it can be concluded that $\text{Si}_5\text{O}_{10}\text{-Ge}_5\text{O}_{10}$ nanocluster might be appropriate candidate for hydrogen storage in transistors. The fluctuation in charge density values demonstrates that the electronic densities were mainly located in the boundary of adsorbate/adsorbent atoms during the adsorption status. As the advantages of lithium over Si/Ge possess its higher electron and hole motion, allowing lithium instruments to operate at higher frequencies than Si/Ge instruments.

Keywords: Lithium battery, $\text{Li}_2[\text{Si}_5\text{O}_{10}\text{-Ge}_5\text{O}_{10}]$, $\text{Si}_5\text{O}_{10}\text{-Ge}_5\text{O}_{10}$, hydrogen storage, DFT.

Corresponding Author: Fateme Mollaamin, Department of Biomedical Engineering, Faculty of Engineering and Architecture, Kastamonu University, Kastamonu, Turkey,
e-mail: fmollaamin@kastamonu.edu.tr, smollaamin@gmail.com

Received: 26 August 2024;

Accepted: 14 October 2024;

Published: 10 December 2024.

1. Introduction

A type of clean fuel is hydrogen that might be employed to accumulate, carry and spread energy produced by other sources and it generates water when applied in a fuel cell (Reza *et al.*, 2021). A fuel cell applies reverse electrolysis to convert an oxidizing agent and hydrogen to power an electric motor (Olabi & Sayed, 2023; Feng *et al.*, 2023; Das *et al.*, 2017).

Carbon nanotubes (CNTs) owing to their lightness, tube construction, vast plane and high reactivity between C and H atoms can be proposed as a promising material for

How to cite (APA):

Mollaamin, F., Monajjemi, M. (2024). Designing novel nanomaterials for Li-ion batteries: A physico-chemical study through hydrogen-powered horizons. *New Materials, Compounds and Applications*, 8(3), 303-323
<https://doi.org/10.62476/nmca83303>

H-grabbing (Lobo *et al.*, 2021; Feng *et al.*, 2023; Mollaamin, 2024; Baughman *et al.*, 2002).

It was investigated that H-storing on C-nano compound indicates the molecular hydrogen dissociation (Yang *et al.*, 2002; Bakshi *et al.*, 2011; Yang *et al.*, 2006; Novoselov *et al.*, 2004). The structure of transition metal-carbon exhibits a charge distribution among boundary atoms and the cationic state of transition metals can be discussed (Geim, 2009; Castro Neto *et al.*, 2009; Mak *et al.*, 2010; Radisavljevic *et al.*, 2011; Rodin *et al.*, 2014). Thus, the electronic charge can be produced through gas molecules adsorption on the surfaces of ionic transition metal (Low *et al.*, 2014; Fei *et al.*, 2014; Ramasubramaniam & Muniz, 2014). Transition metals as dopants might make a whole Hamiltonian perturbation towards alterations in electronic structures, which convert it a substantial usage in magnetic electronic instruments (Yan *et al.*, 2019; Mollaamin & Monajjemi, 2024; Javan, 2016; Wu *et al.*, 2015). Recently, Si-, Ge- or Sn-carbide nanostructures have been suggested as engaged H-grabbing compounds (Nazeer *et al.*, 2018; Zhao *et al.*, 2021; Rong *et al.*, 2016). Since the polarizability of silicon is more than carbon, it is supposed that Si-C/Si nanosheet might attach to compositions more strongly in comparison to the net carbon nano-surfaces (Yodsin *et al.*, 2021; Taha *et al.*, 2023; Monajjemi & Mollaamin, 2024).

H₂ gas is mostly preserved either by liquefaction under high compressing pressure (Mollaamin *et al.*, 2008; Hammad & Dincer, 2018; Monajjemi *et al.*, 2008; Qyyum *et al.*, 2020) or by adsorption on the surface or interstitial region of material cavity (Piñero *et al.*, 2018; Yu *et al.*, 2017; Chettri *et al.*, 2019). In relation to this, the adsorption of H₂ on the surface of two dimensional (2D) materials has advantages in terms of safe functionality and cost-effectiveness. For the effective utilization of H₂ in fuel cells, the adsorption energy and gravimetric weight percentage on the adsorbent should be sufficiently high (Rivard *et al.*, 2019). The adsorption-desorption kinetics and the strength of binding energy ought to be intermediate for hydrogen to bind on the material surfaces with an optimal adsorption energy range.

Moreover, the adsorption and sensing of H₂ and CH₂O molecules on the pristine and transition metal consisting of V, Cr, Mn, Nb, Mo, Tc, Ta, W, or Re doping on B or N site of boron nitride nanosheets. The achieved results exhibit that the pristine boron nitride nanotubes (BNNs) indicate fragile interaction with the H₂ and CH₂O molecules. The H₂ and CH₂O molecules might be strongly adsorption on the transition metal doped BNNs with appreciable adsorption energy through the geometrical deformation on the transition metal doping zone (Thupsuri *et al.*, 2021).

In our previous works, the investigation of energy storage in fuel cells through hydrogen adsorption has been accomplished using DFT calculations through different nanomaterials consisting of silicon/germanium/tin/lead nano-carbides (Mollaamin & Monajjemi, 2024), magnesium-aluminum alloy (Mollaamin *et al.*, 2024) and aluminum/carbon/ silicon doping boron nitride nanocage (Mollaamin, 2024).

Nanomaterials with remarkable specific structures indicate promising applications in the field of energy storage, electrocatalysis and fuel cells. This article wants to demonstrate a facile approach for fabricating nanocluster of Si₅O₁₀-Ge₅O₁₀ as a template at a moderate condition for hydrogen storage.

Currently, the present research aims to explore the possibility of using Si₅O₁₀-Ge₅O₁₀ nanocluster for hydrogen storage by employing first-principles calculations. We have analyzed the structural and electronic properties of Si₅O₁₀, Ge₅O₁₀, Si₅O₁₀-Ge₅O₁₀,

$\text{Li}_2[\text{Si}_5\text{O}_{10}\text{-Ge}_5\text{O}_{10}]$ and hydrated nanocluster of $\text{H}_2[\text{Si}_5\text{O}_{10}\text{-Ge}_5\text{O}_{10}]$ and $\text{Li}_2\text{H}_4[\text{Si}_5\text{O}_{10}\text{-Ge}_5\text{O}_{10}]$ using state-of-the-art computational techniques.

2. Materials and Methods

The aim of this study is to hydrogen adsorption by using Si_5O_{10} , Ge_5O_{10} , $\text{Si}_5\text{O}_{10}\text{-Ge}_5\text{O}_{10}$ nanoclusters (Figure 1). Hydrated nanocluster of $\text{H}_2[\text{Si}_5\text{O}_{10}\text{-Ge}_5\text{O}_{10}]$ and $\text{Li}_2\text{H}_4[\text{Si}_5\text{O}_{10}\text{-Ge}_5\text{O}_{10}]$ were modeled in the presence of Si_5O_{10} , Ge_5O_{10} and production of $\text{Si}_5\text{O}_{10}\text{-Ge}_5\text{O}_{10}$ and $\text{Li}_2[\text{Si}_5\text{O}_{10}\text{-Ge}_5\text{O}_{10}]$ which can increase the hydrogen storage in semiconductor transistors. In DFT, as it is used for computational chemistry, the hybrid functional Becke 3-parameter Lee-Yang-Parr (B3LYP) appears to offer the greatest contribution. A new hybrid exchange-correlation functional named Coulomb-Attenuating method with B3LYP (CAM-B3LYP) is proposed which combines the hybrid qualities of B3LYP and the long-range correction (Yanai *et al.*, 2004).

Besides, in the DFT-D3 method of Grimme *et al.* (2010) the following expression for the Van Der Waals (VDW)-dispersion energy-correction term is used:

$$E_{\text{disp}} = -\frac{1}{2} \sum_{i=1}^{N_{\text{at}}} \sum_{j=1}^{N_{\text{at}}} \sum_L \left(f_{d,6} (r_{ij,L}) \frac{C_{6ij}}{r_{ij,L}^6} + f_{d,8} (r_{ij,L}) \frac{C_{8ij}}{r_{ij,L}^8} \right) \quad (1)$$

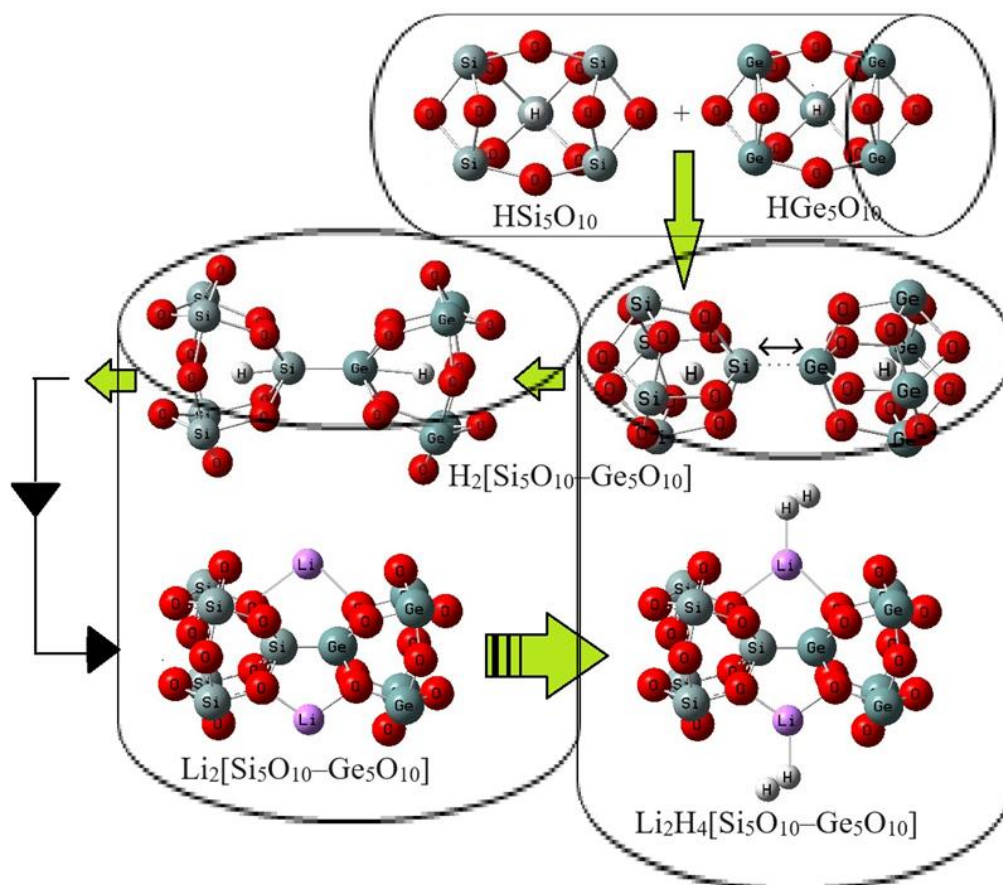


Figure 1. Application of $\text{Si}_5\text{O}_{10}\text{-Ge}_5\text{O}_{10}$ for increasing hydrogen adsorption towards the energy storage in transistors accompanying formation of hydrated nanoclusters including $\text{HSi}_5\text{O}_{10}$, $\text{HGe}_5\text{O}_{10}$, $\text{H}_2[\text{Si}_5\text{O}_{10}\text{-Ge}_5\text{O}_{10}]$ and $\text{Li}_2\text{H}_4[\text{Si}_5\text{O}_{10}\text{-Ge}_5\text{O}_{10}]$ using CAM-B3LYP-D3/6-311+G (d,p) calculation

The dispersion coefficients C_{6ij} are geometry dependent as they are adjusted based on the local geometry (coordination number) around atoms i and j . Besides, Electron Paramagnetic Resonance (EPR) has been done which is a method for studying materials with unpaired electrons. The basic concepts of EPR are analogous to those of NMR, but the spins excited are those of the electrons instead of the atomic nuclei (Zavoisky, 1945). Therefore, in our research, the calculations have been done through CAM-B3LYP-D3/EPR-3 level of theory.

Figure 1 has shown the process of hydrogen adsorption on $\text{Si}_5\text{O}_{10}\text{-Ge}_5\text{O}_{10}$ surface which includes the formation of hydrated nanoclusters containing $\text{H-Si}_5\text{O}_{10}$, $\text{H-Ge}_5\text{O}_{10}$, $\text{H-Si}_5\text{O}_{10}\text{-Ge}_5\text{O}_{10}\text{-H}$. The Bader charge analysis (Henkelman *et al.*, 2006) was discussed during trapping of hydrogen atoms by $\text{Si}_5\text{O}_{10}\text{-Ge}_5\text{O}_{10}$ and formation of $\text{HSi}_5\text{O}_{10}$, $\text{HGe}_5\text{O}_{10}$, $\text{H}_2[\text{Si}_5\text{O}_{10}\text{-Ge}_5\text{O}_{10}]$ and $\text{Li}_2\text{H}_4[\text{Si}_5\text{O}_{10}\text{-Ge}_5\text{O}_{10}]$ nanoclusters (Figure 1). The rigid potential energy surface using density functional theory (Blöchl, 1994; Perdew *et al.*, 1996; Ziesche *et al.*, 1998; Arrigoni & Madsen, 2019; Hohenberg & Kohn, 1964; Kohn & Sham, 1965; Becke, 1993; Lee *et al.*, 1988; Kim & Jordan, 1994; Stephens *et al.*, 1994; Cramer, 2013; Mollaamin & Monajjemi, 2024; Mollaamin & Monajjemi, 2023; Vosko *et al.*, 1980) was performed due to Gaussian 16 revision C.01 program package (Frisch *et al.*, 2016) and GaussView 6.1 (Dennington *et al.*, 2016). The coordination input for hydrogen grabbing by $\text{Si}_5\text{O}_{10}\text{-Ge}_5\text{O}_{10}$ and $\text{Li}_2[\text{Si}_5\text{O}_{10}\text{-Ge}_5\text{O}_{10}]$ has applied 6-311+G (d,p) and EPR-3 basis sets.

3. Results and Discussion

3.1. Theory of Nuclear quadrupole resonance (NQR)

The NQR frequencies have been measured for Si_5O_{10} , $\text{HSi}_5\text{O}_{10}$, Ge_5O_{10} and $\text{HGe}_5\text{O}_{10}$ towards estimating the hydrated nanocluster of $\text{H}_2[\text{Si}_5\text{O}_{10}\text{-Ge}_5\text{O}_{10}]$ (Table 1). The NQR method is related to the multipole expansion in Cartesian coordinates as the Equation (1) (Trontelj *et al.*, 2020; Sciotto *et al.*, 2024):

$$V(r) = V(0) + \left[\left(\frac{\partial V}{\partial x_i} \right) \Big|_0 \cdot x_i \right] + \frac{1}{2} \left[\left(\frac{\partial^2 V}{\partial x_i \partial x_j} \right) \Big|_0 \cdot x_i x_j \right] + \dots \quad (2)$$

After that, a simplification on the equation (6), there are only the second derivatives related to the identical variable for the potential energy (Trontelj *et al.*, 2020; Sciotto *et al.*, 2024):

$$U = -\frac{1}{2} \int_{\mathcal{D}} d^3 r \rho_r \left[\left(\frac{\partial^2 V}{\partial x_i^2} \right) \Big|_0 \cdot x_i^2 \right] = -\frac{1}{2} \int_{\mathcal{D}} d^3 r \rho_r \left[\left(\frac{\partial E_i}{\partial x_i} \right) \Big|_0 \cdot x_i^2 \right] = -\frac{1}{2} \left(\frac{\partial E_i}{\partial x_i} \right) \Big|_0 \cdot \int_{\mathcal{D}} d^3 r [\rho(r) \cdot x_i^2]. \quad (3)$$

There are two parameters which must be gotten from NQR experiments: the quadrupole coupling constant, χ and asymmetry parameter of the EFG tensor η :

$$\chi = \frac{e^2 Q q_{zz}}{h}, \quad (4)$$

$$\eta = \frac{q_{xx} - q_{yy}}{q_{zz}}, \quad (5)$$

where q_{ii} are ingredients of the EFG tensor at the quadrupole nucleus determined in the EFG principal axes system, Q is the nuclear quadrupole moment, e is the proton charge and h is the Planck's constant (Luo *et al.*, 2020; Young *et al.*, 2008).

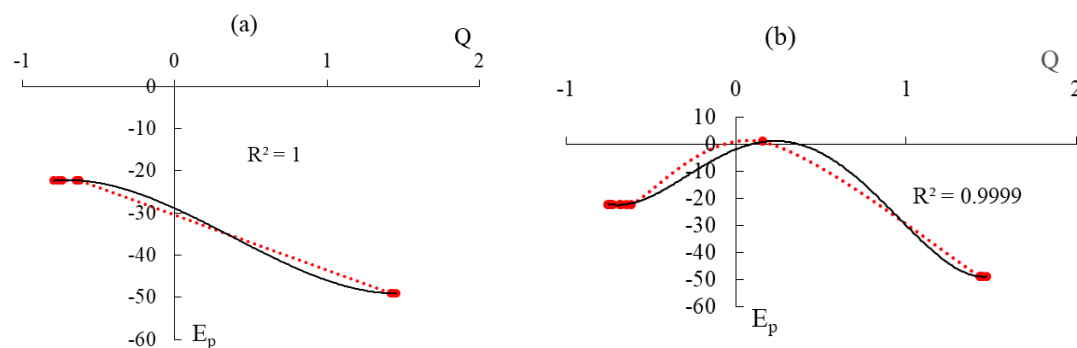
In this research work, the electric potential as the quantity of work energy through carrying over the electric charge from one position to another position in the essence of electric field has been evaluated for Si_5O_{10} , $\text{HSi}_5\text{O}_{10}$, Ge_5O_{10} and $\text{HGe}_5\text{O}_{10}$ complexes (Table 1).

Table 1. The electric potential (E_p /a.u.) and Bader charge (Q /coulomb) through NQR calculation for Si_5O_{10} , $\text{HSi}_5\text{O}_{10}$, Ge_5O_{10} and $\text{HGe}_5\text{O}_{10}$ complexes

Si_5O_{10}			$\text{HSi}_5\text{O}_{10}$			Ge_5O_{10}			$\text{HGe}_5\text{O}_{10}$		
Atom	Q	E_p	Atom	Q	E_p	Atom	Q	E_p	Atom	Q	E_p
Si(1)	1.42	-49.09	Si(1)	1.44	-49.08	Ge(1)	1.49	-155.04	Ge(1)	1.52	-155.04
O(2)	-0.62	-22.29	O(2)	-0.61	-22.30	O(2)	-0.66	-22.31	O(2)	-0.65	-22.32
O(3)	-0.79	-22.33	O(3)	-0.75	-22.31	O(3)	-0.83	-22.35	O(3)	-0.78	-22.33
Si(4)	1.42	-49.09	Si(4)	1.43	-49.09	Ge(4)	1.50	-155.05	Ge(4)	1.51	-155.04
Si(5)	1.42	-49.09	Si(5)	1.44	-49.09	Ge(5)	1.49	-155.05	Ge(5)	1.52	-155.04
Si(6)	1.42	-49.09	Si(6)	1.43	-49.10	Ge(6)	1.49	-155.05	Ge(6)	1.51	-155.04
O(7)	-0.65	-22.30	O(7)	-0.68	-22.33	O(7)	-0.68	-22.320	O(7)	-0.72	-22.34
O(8)	-0.79	-22.33	O(8)	-0.74	-22.30	O(8)	-0.83	-22.35	O(8)	-0.77	-22.32
O(9)	-0.74	-22.31	O(9)	-0.74	-22.32	O(9)	-0.77	-22.33	O(9)	-0.78	-22.34
O(10)	-0.76	-22.34	O(10)	-0.74	-22.32	O(10)	-0.80	-22.36	O(10)	-0.78	-22.35
O(11)	-0.76	-22.34	O(11)	-0.73	-22.34	O(11)	-0.80	-22.36	O(11)	-0.78	-22.36
O(12)	-0.74	-22.31	O(12)	-0.73	-22.32	O(12)	-0.78	-22.33	O(12)	-0.76	-22.34
Si(13)	1.45	-49.09	Si(13)	1.47	-49.08	Ge(13)	1.53	-155.05	Ge(13)	1.56	-155.04
O(14)	-0.64	-22.30	O(14)	-0.64	-22.30	O(14)	-0.67	-22.31	O(14)	-0.70	-22.34
O(15)	-0.63	-22.29	O(15)	-0.70	-22.34	O(15)	-0.66	-22.31	O(15)	-0.69	-22.35
			H(16)	-0.15	-0.770				H(16)	-0.20	-0.784

Si, Ge, O and hydrogen atoms absorbed on Si_5O_{10} and Ge_5O_{10} have been calculated through the Bader charge and electronic potential properties. The values detect that with augmenting the negative charge of various atoms, the electric potential extracted from NQR calculations grows. Besides, the elements of O (2), O (3), O (7), O (8), O (9), O (10), O (11), O (12), O (14), O (15) of Si_5O_{10} and Ge_5O_{10} have exhibited the most efficiency for admitting the electron from electron donor of H (16) adsorbed on Si_5O_{10} and Ge_5O_{10} (Table 1).

In Figure 2 (a-d), it has been sketched the electric potential of nuclear quadrupole resonance versus Bader charge for some atoms of Si, Ge, O and hydrogen atoms absorbed on Si_5O_{10} and Ge_5O_{10} .



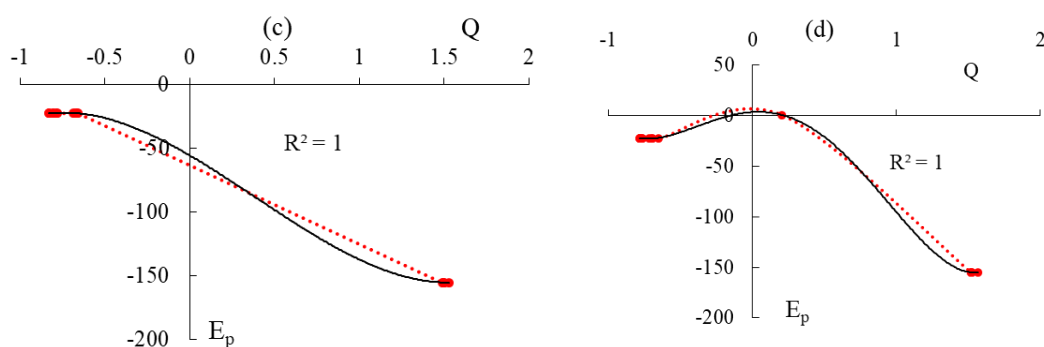


Figure 2. Electric potential (a.u.) versus Bader charge (coulomb) through NQR calculation for (a) Si_5O_{10} , (b) $\text{HSi}_5\text{O}_{10}$, (c) Ge_5O_{10} and (d) $\text{HGe}_5\text{O}_{10}$

In Figure 2a, it was observed the behavior of Si and O atoms in Si_5O_{10} with high sensitivity based on relation coefficient of $R^2 = 0.9999$; however, hydrogen adsorption on the Si_5O_{10} ($\text{HSi}_5\text{O}_{10}$) has shown high sensitivity with relation coefficient of $R^2 = 0.9999$ (Figure 2b). In Figure 2c, it was observed the behavior of Ge and O atoms in Ge_5O_{10} and hydrogen adsorption on the Ge_5O_{10} ($\text{HGe}_5\text{O}_{10}$) (Figure 2d) with high sensitivity of $R^2 = 1$. The fluctuated peaks for electric potential have been shown around hydrogen adsorption on the Si_5O_{10} and Ge_5O_{10} which demonstrates the electron accepting specifications of hydrogen versus the Si, Ge, O of Si_5O_{10} and Ge_5O_{10} (Figure 2a, 2d). Besides, it can be considered that oxygen atoms in the functionalized Si_5O_{10} and Ge_5O_{10} might have more impressive sensitivity for accepting the electrons from H atoms in the process of adsorption mechanism. Based on the mentioned results, there can be renewed interest in combination of silicon and germanium as a nanocluster of Si_5O_{10} – Ge_5O_{10} for potential applications in next-generation electronics.

3.2. Analysis of Nuclear Magnetic Resonance spectra

Based on the resulted amounts, nuclear magnetic resonance (NMR) spectra of Si_5O_{10} and Ge_5O_{10} complexes as the potential molecules for hydrogen storage can unravel the efficiency of these complexes for saving clean energy. From the DFT calculations, it has been attained the chemical shielding (CS) tensors in the principal axes system to estimate the isotropic chemical-shielding (CSI) and anisotropic chemical-shielding (CSA) (Sohail *et al.*, 2023):

$$\sigma_{iso} = (\sigma_{11} + \sigma_{22} + \sigma_{33})/3, \quad (6)$$

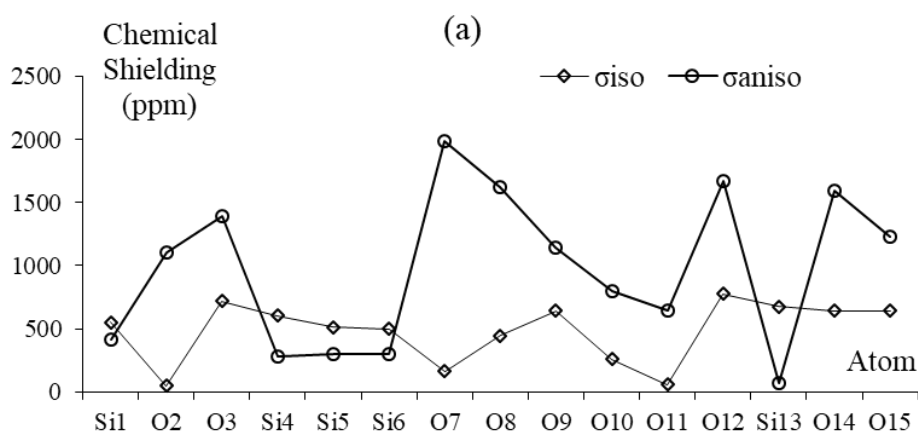
$$\sigma_{aniso} = \sigma_{33} - \frac{\sigma_{22} + \sigma_{11}}{2}. \quad (7)$$

The NMR data of isotropic (σ_{iso}) and anisotropic shielding tensors (σ_{aniso}) of hydrogen atoms adsorbed on Si_5O_{10} and Ge_5O_{10} complexes towards formation of $\text{HSi}_5\text{O}_{10}$ and $\text{HGe}_5\text{O}_{10}$ complexes have been computed by Gaussian 16 revision C.01 program package (Dennington *et al.*, 2016) and been shown in Table 2.

Table 2. Data of NMR shielding tensors (ppm) for selected atoms of Si_5O_{10} , $\text{HSi}_5\text{O}_{10}$, Ge_5O_{10} and $\text{HGe}_5\text{O}_{10}$ complexes

Si_5O_{10}			$\text{HSi}_5\text{O}_{10}$			Ge_5O_{10}			$\text{HGe}_5\text{O}_{10}$		
Atom	σ_{iso}	σ_{aniso}	Atom	σ_{iso}	σ_{aniso}	Atom	σ_{iso}	σ_{aniso}	Atom	σ_{iso}	σ_{aniso}
Si(1)	554.06	419.08	Si(1)	636.08	83.31	Ge(1)	11774.57	78310.40	Ge(1)	2269.96	265.46
O(2)	48.40	1103.17	O(2)	197.71	180.52	O(2)	7981.03	45129.91	O(2)	185.77	323.78
O(3)	719.20	1393.84	O(3)	213.90	571.64	O(3)	26849.60	102235.88	O(3)	235.00	690.97
Si(4)	606.85	283.53	Si(4)	612.49	136.09	Ge(4)	2860.04	56431.23	Ge(4)	2254.92	354.40
Si(5)	515.08	300.30	Si(5)	590.56	112.09	Ge(5)	22560.33	50034.95	Ge(5)	2196.23	239.01
Si(6)	499.44	298.51	Si(6)	640.61	109.00	Ge(6)	25249.19	67283.27	Ge(6)	2283.05	294.68
O(7)	165.28	1989.85	O(7)	257.47	540.46	O(7)	28391.88	116633.36	O(7)	192.29	265.99
O(8)	446.38	1626.01	O(8)	345.30	760.80	O(8)	19250.32	151688.34	O(8)	400.69	945.35
O(9)	644.00	1145.01	O(9)	396.42	516.76	O(9)	8016.65	16619.93	O(9)	429.44	692.57
O(10)	258.21	801.06	O(10)	291.98	500.11	O(10)	12714.21	20281.55	O(10)	322.30	641.07
O(11)	59.31	646.45	O(11)	381.78	579.44	O(11)	9151.57	14760.91	O(11)	363.38	661.78
O(12)	777.76	1673.73	O(12)	592.90	761.13	O(12)	45077.01	82973.35	O(12)	644.30	1039.24
Si(13)	676.74	69.96	Si(13)	700.35	80.46	Ge(13)	1836.03	6719.10	Ge(13)	2377.42	144.00
O(14)	644.64	1598.29	O(14)	192.65	365.70	O(14)	21908.37	61863.15	O(14)	93.65	302.72
O(15)	640.66	1233.63	O(15)	575.73	737.13	O(15)	6288.94	33932.60	O(15)	458.00	712.97
			H(16)	33.88	5.14				H(16)	38.01	2.78

In Table 2, NMR data has reported the notable amounts for hydrogen atoms which were adsorbed on Si_5O_{10} and Ge_5O_{10} complexes. The observed increase in the chemical shift anisotropy spans for H atoms adsorption on Si_5O_{10} and Ge_5O_{10} complexes are near O (2), O (3), O (7), O (8), O (12), O (14) and O (15). The notable fragile signal intensity close to the parallel edge of the nanocluster sample might be owing to silicon or germanium binding induced non-spherical distribution of these clusters. Figure 3 (a-d) exhibited the same tendency of shielding for silicon or germanium; however, a considerable deviation exists from doping atoms of O (2), O (3), O (7), O (8), O (12), O (14) and O (15) through interaction with hydrogen atoms during adsorbing on Si_5O_{10} and Ge_5O_{10} complexes.



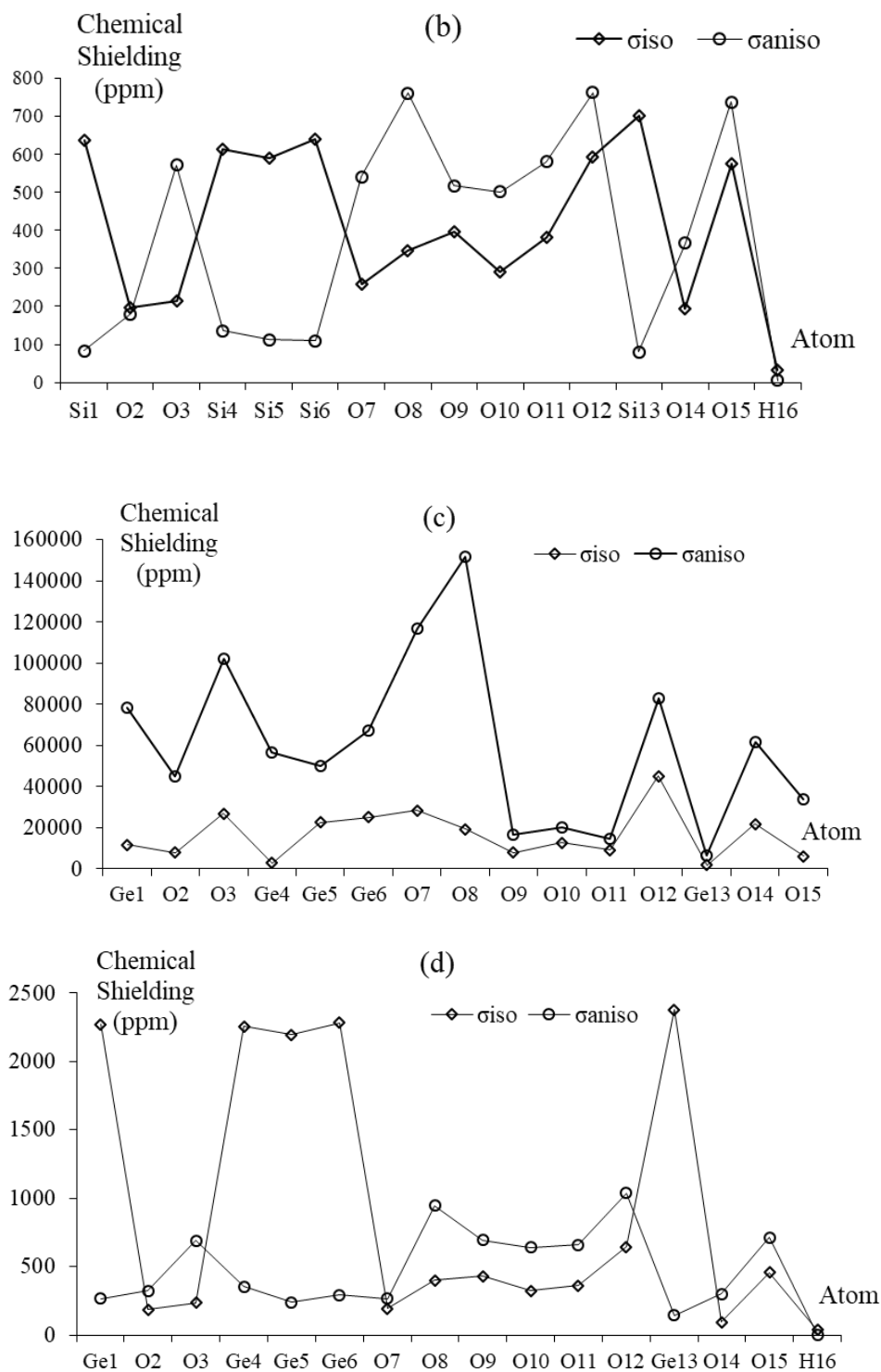


Figure 3. The NMR spectra for (a) Si_5O_{10} , (b) HSi_5O_{10} , (c) Ge_5O_{10} and (d) HGe_5O_{10} complexes

NMR spectroscopy has shown the gap chemical shielding between silicon and oxygen in Si_5O_{10} (Figure 3a), hydrogen, silicon and oxygen in HSi_5O_{10} (Figure 3b), germanium and oxygen in Ge_5O_{10} (Figure 3c), hydrogen, germanium and oxygen in HGe_5O_{10} (Figure 3d). The yield of electromagnetic shifting can be directed by oxygen

atoms of O (3), O (7), O (12), O (14) in Si_5O_{10} (Figure 3a), O (3), O (8), O (12), O (15) in $\text{HSi}_5\text{O}_{10}$ (Figure 3b), O (3), O (8), O (12), O (14) in Ge_5O_{10} (Figure 3c) and Ge (1), Ge (4), Ge (5), Ge (6), Ge (13) in $\text{HGe}_5\text{O}_{10}$ (Figure 3d). The results have shown that the intensity for hydrogen adsorption can be developed in Ge_5O_{10} through germanium atoms compared to silicon atoms in Si_5O_{10} . Although both silicon and germanium are semiconductor elements, germanium can be more conductive than silicon in transistors due to high semiconducting properties. Therefore, it can be promised that the adapted outcomes would be advantageous in modelling a novel $\text{Si}_5\text{O}_{10}\text{-Ge}_5\text{O}_{10}$ complex for increasing the adsorption of hydrogen atoms in transistors based on their structural studies.

3.3. Atomic charge distribution

Atomic charge was discussed during trapping of hydrogens by $\text{Si}_5\text{O}_{10}\text{-Ge}_5\text{O}_{10}$ and $\text{Li}_2[\text{Si}_5\text{O}_{10}\text{-Ge}_5\text{O}_{10}]$ nanoclusters towards formation of $\text{H}_2[\text{Si}_5\text{O}_{10}\text{-Ge}_5\text{O}_{10}]$ and $\text{Li}_2\text{H}_4[\text{Si}_5\text{O}_{10}\text{-Ge}_5\text{O}_{10}]$ nanoclusters, respectively (Table 3).

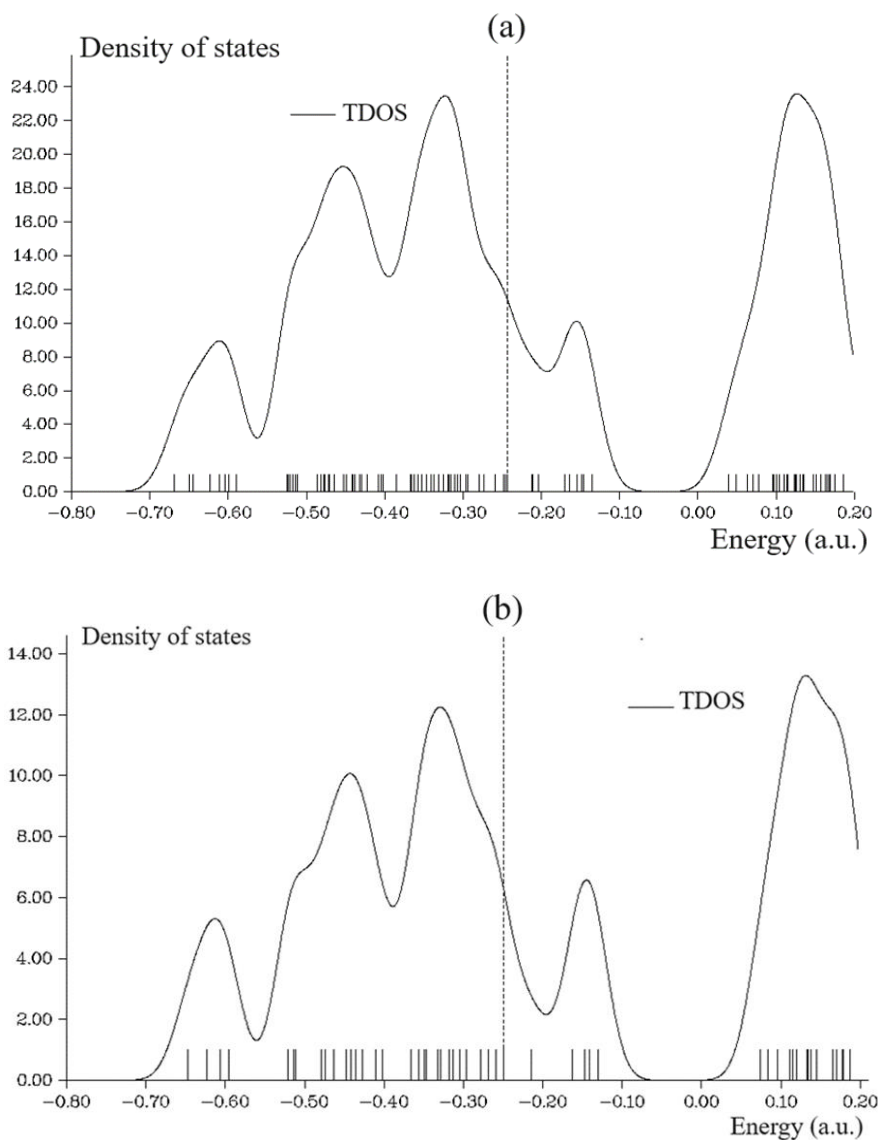
Table 3. The atomic charge (Q/coulomb) for $\text{Si}_5\text{O}_{10}\text{-Ge}_5\text{O}_{10}$, $\text{H}_2[\text{Si}_5\text{O}_{10}\text{-Ge}_5\text{O}_{10}]$, $\text{Li}_2[\text{Si}_5\text{O}_{10}\text{-Ge}_5\text{O}_{10}]$ and $\text{Li}_2\text{H}_4[\text{Si}_5\text{O}_{10}\text{-Ge}_5\text{O}_{10}]$ nanoclusters

$\text{Si}_5\text{O}_{10}\text{-Ge}_5\text{O}_{10}$		$\text{H}_2[\text{Si}_5\text{O}_{10}\text{-Ge}_5\text{O}_{10}]$		$\text{Li}_2[\text{Si}_5\text{O}_{10}\text{-Ge}_5\text{O}_{10}]$		$\text{Li}_2\text{H}_4[\text{Si}_5\text{O}_{10}\text{-Ge}_5\text{O}_{10}]$	
Atom	Charge	Atom	Charge	Atom	Charge	Atom	Charge
Si(1)	1.49	Si(1)	1.43	Si(1)	1.46	Si(1)	1.45
O(2)	-0.63	O(2)	-0.64	O(2)	-0.68	O(2)	-0.65
O(3)	-0.80	O(3)	-0.79	O(3)	-0.83	O(3)	-0.83
Si(4)	1.46	Si(4)	1.41	Si(4)	1.43	Si(4)	1.43
Si(5)	1.46	Si(5)	1.42	Si(5)	1.46	Si(5)	1.44
Si(6)	1.47	Si(6)	1.44	Si(6)	1.46	Si(6)	1.46
O(7)	-0.66	O(7)	-0.67	O(7)	-0.65	O(7)	-0.68
O(8)	-0.78	O(8)	-0.80	O(8)	-0.83	O(8)	-0.84
O(9)	-0.71	O(9)	-0.72	O(9)	-0.80	O(9)	-0.78
O(10)	-0.75	O(10)	-0.70	O(10)	-1.01	O(10)	-1.00
O(11)	-0.76	O(11)	-0.76	O(11)	-0.80	O(11)	-0.80
O(12)	-0.72	O(12)	-0.73	O(12)	-0.94	O(12)	-0.95
Si(13)	0.99	Si(13)	0.85	Si(13)	1.63	Si(13)	1.63
O(14)	-0.66	O(14)	-0.68	O(14)	-0.70	O(14)	-0.73
O(15)	-0.63	O(15)	-0.64	O(15)	-0.76	O(15)	-0.72
Ge(16)	1.57	Ge(16)	1.55	Ge(16)	1.39	Ge(16)	1.41
O(17)	-0.68	O(17)	-0.70	O(17)	-0.67	O(17)	-0.65
O(18)	-0.83	O(18)	-0.79	O(18)	-0.78	O(18)	-0.78
Ge(19)	1.56	Ge(19)	1.55	Ge(19)	1.38	Ge(19)	1.39
Ge(20)	1.55	Ge(20)	1.55	Ge(20)	1.39	Ge(20)	1.39
Ge(21)	1.57	Ge(21)	1.55	Ge(21)	1.39	Ge(21)	1.40
O(22)	-0.72	O(22)	-0.73	O(22)	-0.62	O(22)	-0.67
O(23)	-0.81	O(23)	-0.77	O(23)	-0.78	O(23)	-0.78
O(24)	-0.75	O(24)	-0.80	O(24)	-0.94	O(24)	-0.94
O(25)	-0.81	O(25)	-0.79	O(25)	-0.80	O(25)	-0.77
O(26)	-0.80	O(26)	-0.80	O(26)	-0.92	O(26)	-0.90
O(27)	-0.76	O(27)	-0.78	O(27)	-0.77	O(27)	-0.79
Ge(28)	1.54	Ge(28)	2.27	Ge(28)	1.24	Ge(28)	1.25
O(29)	-0.70	O(29)	-0.72	O(29)	-0.69	O(29)	-0.73
O(30)	-0.67	O(30)	-0.70	O(30)	-0.73	O(30)	-0.72
		H(31)	-0.13	Li(31)	0.73	Li(31)	0.64
		H(32)	-0.13	Li(32)	0.75	Li(32)	0.64
						H(33)	-0.02
						H34	-0.00
						H35	0.12
						H36	0.10

Atomic charge of Si, Ge, O, Li and hydrogen atoms absorbed on $\text{Si}_5\text{O}_{10}\text{-Ge}_5\text{O}_{10}$ and $\text{Li}_2[\text{Si}_5\text{O}_{10}\text{-Ge}_5\text{O}_{10}]$ have been measured. The values detect that with adding lithium, the negative atomic charge of oxygen atoms of O (9), O (10), O (11), O (12), O (24), O (25), O (26), O (27) in $\text{Li}_2[\text{Si}_5\text{O}_{10}\text{-Ge}_5\text{O}_{10}]$ augments. In fact, $\text{Li}_2[\text{Si}_5\text{O}_{10}\text{-Ge}_5\text{O}_{10}]$ has shown more efficiency than $\text{Si}_5\text{O}_{10}\text{-Ge}_5\text{O}_{10}$ for admitting the electron from electron donor of H (33), H (34), H (35) and H (36) (Table 3).

3.4. TDOS analysis

Squirming the molecular orbital data owing to gaussian graphs of unit altitude and entire width at half maximum (FWHM) of 0.3 eV by GaussSum 3.0.2 (O'boyle *et al.*, 2008) have computed total density of states (TDOS) diagrams. To better understand the adsorption characteristics of hydrogen by $\text{Si}_5\text{O}_{10}\text{-Ge}_5\text{O}_{10}$, $\text{H}_2[\text{Si}_5\text{O}_{10}\text{-Ge}_5\text{O}_{10}]$, $\text{Li}_2[\text{Si}_5\text{O}_{10}\text{-Ge}_5\text{O}_{10}]$ and $\text{Li}_2\text{H}_4[\text{Si}_5\text{O}_{10}\text{-Ge}_5\text{O}_{10}]$ nanoclusters, TDOS has been measured. This parameter can indicate the existence of important chemical interactions often on the convex side (Figure 5a-d).



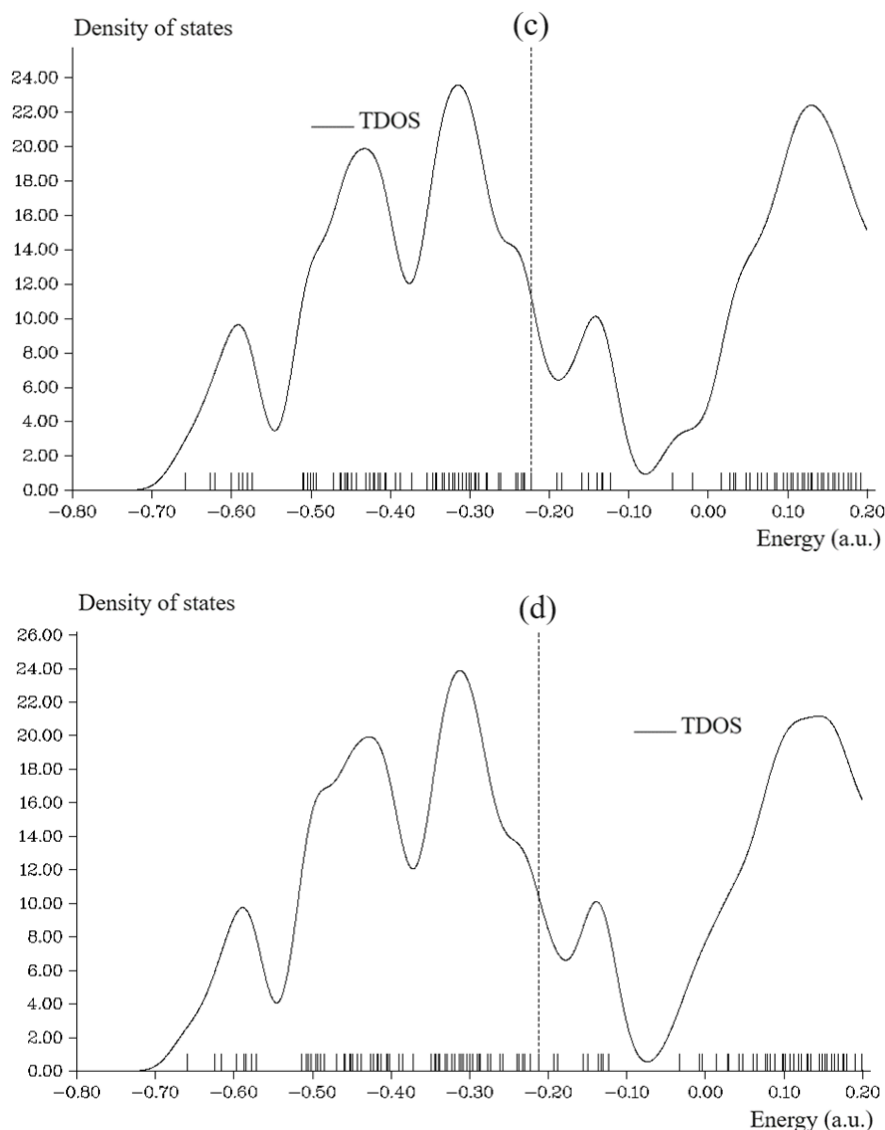


Figure 5. TDOS graphs of (a) $\text{Si}_5\text{O}_{10}\text{-Ge}_5\text{O}_{10}$, (b) $\text{H}_2[\text{Si}_5\text{O}_{10}\text{-Ge}_5\text{O}_{10}]$, (c) $\text{Li}_2[\text{Si}_5\text{O}_{10}\text{-Ge}_5\text{O}_{10}]$ and (d) $\text{Li}_2\text{H}_4[\text{Si}_5\text{O}_{10}\text{-Ge}_5\text{O}_{10}]$ nanoclusters

During formation of $\text{Si}_5\text{O}_{10}\text{-Ge}_5\text{O}_{10}$ cluster, Figure 5a has shown sharp and sophisticated peaks around -0.3 , -0.45 and -0.65 a.u. due to covalent bond between two crystals of Si_5O_{10} and Ge_5O_{10} . However, after H-grabbing by $\text{Si}_5\text{O}_{10}\text{-Ge}_5\text{O}_{10}$ cluster, Figure 5b has represented sharp and sophisticated peaks for the hydrated cluster of $\text{H}_2[\text{Si}_5\text{O}_{10}\text{-Ge}_5\text{O}_{10}]$ around -0.32 and -0.45 a.u. In Figure 3c, $\text{Li}_2[\text{Si}_5\text{O}_{10}\text{-Ge}_5\text{O}_{10}]$ has shown two pointed peaks around -0.32 , -0.45 a.u. After H-grabbing by $\text{Li}_2[\text{Si}_5\text{O}_{10}\text{-Ge}_5\text{O}_{10}]$ and formation of $\text{H}_4[\text{Si}_5\text{O}_{10}\text{-Ge}_5\text{O}_{10}]$ complex, the two-pointed peaks have been shifted to -0.30 and -0.42 a.u. (Figure 3d). The maximum energy of TDOS for $\text{Li}_2[\text{Si}_5\text{O}_{10}\text{-Ge}_5\text{O}_{10}]$ (Figure 5c) with three sharp peaks around -0.35 , -0.45 and -0.65 a.u. with maximum density of state around -0.35 a.u. has been shown. Moreover, the similar amounts of TDOS for $\text{Li}_2\text{H}_4[\text{Si}_5\text{O}_{10}\text{-Ge}_5\text{O}_{10}]$ (Figure 5d) through some fluctuations in the behavior of the graphs have been observed.

3.5. LOL analysis

Localized orbital locator (LOL) has a similar expression compared to electron localization function (ELF) (Schmider & Becke, 2000).

$$\text{LOL}(\mathbf{r}) = \frac{\tau(\mathbf{r})}{1+\tau(\mathbf{r})} \quad ; \quad \tau(\mathbf{r}) = \frac{D_0(\mathbf{r})}{\frac{1}{2} \sum_i \eta_i |\nabla \varphi_i(\mathbf{r})|^2}, \quad (8)$$

$$D_0(\mathbf{r}) = \frac{3}{10} (6\pi^2)^{2/3} [\rho_\alpha(\mathbf{r})^{5/3} + \rho_\beta(\mathbf{r})^{5/3}] \quad (9)$$

The chemically significant regions that are highlighted by LOL and ELF are generally qualitative comparable, while Jacobsen (2008) pointed out that LOL conveys a more decisive and clearer picture than ELF. Obviously, LOL can be interpreted in kinetic energy way as for ELF, however LOL can also be interpreted in view of localized orbital. Small or large LOL value usually appears in boundary or inner region of localized orbitals because the gradient of orbital wavefunction is large or small in this area. The value range of LOL is identical to ELF, namely [0,1].

Multiwfn (Arrigoni & Madsen, 2019) also supports the approximate version of LOL defined by Tsirelson and Stash (2002), namely the actual kinetic energy term in LOL is replaced by second-order gradient expansion like ELF which may demonstrate a broad span of bonding samples. This Tsirelson's version of LOL can be activated by setting "ELFLOL_type" to 1. For special reason, if "ELFLOL_type" in settings.ini is changed from 0 to 2, another formalism will be used:

$$\text{LOL}(\mathbf{r}) = \frac{1}{1 + [1/\tau(\mathbf{r})]^2}. \quad (10)$$

If the parameter "ELFLOL_cut" in settings.ini is set to x , then LOL will be zero where LOL is less than x .

Nevertheless, the distinction between deduced/raised electron delocalization/localization into cyclic π -conjugated sets stays encouraging for ELF (Matta *et al.*, 2004). The grosser the electron localization is in an area, the more likely the electron movement is restricted within it. Therefore, they might be discerned from the ones away if electrons are totally centralized. As Bader investigated, the zones with large electron localization possess extensive magnitudes of Fermi hole integration. But, with having a six-dimension function for the Fermi hole, it seems hard to be studied directly. Then, Becke and Edgecombe remarked that spherically averaged like spin conditional pair probability possesses a direct correlation with the Fermi hole and proposed the parameter of electron localization function (ELF) in Multiwfn program (Arrigoni & Madsen, 2019) and popularized for spin-polarized procedure (Tian & Feiwu, 2011):

$$\text{ELF}(\mathbf{r}) = \frac{1}{1 + [D(\mathbf{r})/D_0(\mathbf{r})]}, \quad (11)$$

where

$$D(\mathbf{r}) = \frac{1}{2} \sum_i \eta_i |\nabla \varphi_i(\mathbf{r})|^2 - \frac{1}{8} \left[\frac{|\nabla \rho_\alpha(\mathbf{r})|^2}{\rho_\alpha(\mathbf{r})} + \frac{|\nabla \rho_\beta(\mathbf{r})|^2}{\rho_\beta(\mathbf{r})} \right] \quad (12)$$

and

$$D_0(\mathbf{r}) = \frac{3}{10} (6\pi^2)^{2/3} [\rho_\alpha(\mathbf{r})^{5/3} + \rho_\beta(\mathbf{r})^{5/3}]. \quad (13)$$

For close-shell system, since $\rho_\alpha = \rho_\beta = (1/2)\rho$, D and D_0 terms can be simplified as:

$$D(\mathbf{r}) = \frac{1}{2} \sum_i \eta_i |\nabla \varphi_i(\mathbf{r})|^2 - \frac{1}{8} \frac{|\nabla \rho(\mathbf{r})|^2}{\rho(\mathbf{r})} \quad (14)$$

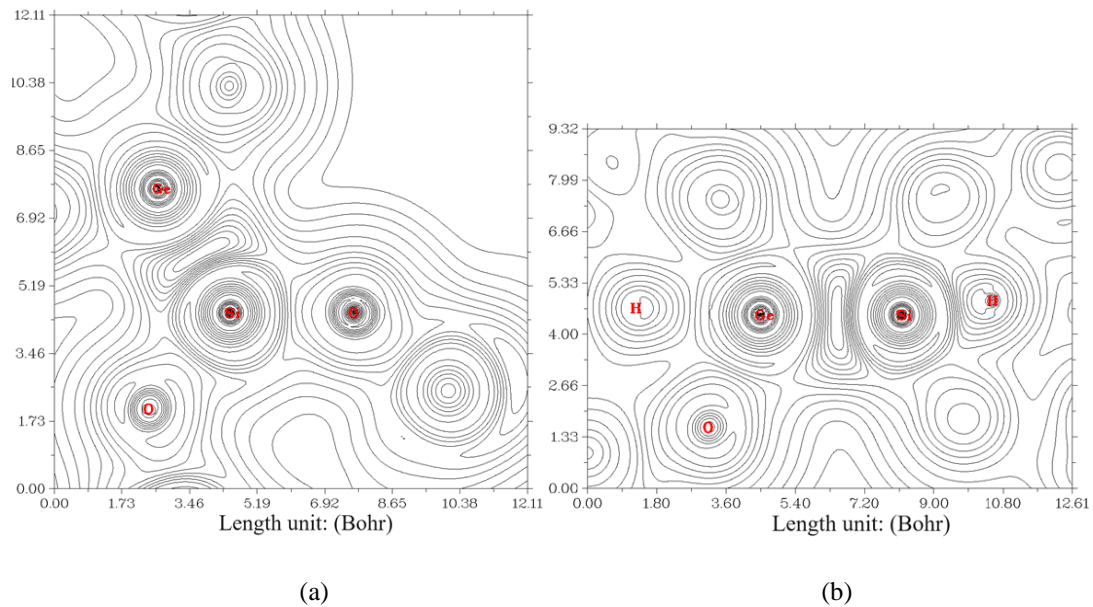
and

$$D_0(\mathbf{r}) = (3/10)(3\pi^2)^{2/3} \rho(\mathbf{r})^{5/3}. \quad (15)$$

Regarding kinetic energy, ELF was rechecked to be more punctual for both Kohn-Sham DFT and post-HF wavefunctions (Savin *et al.*, 1992). In fact, the excess kinetic energy density caused by Pauli repulsion was unfolded by $D(\mathbf{r})$ and $D_0(\mathbf{r})$ may be inspected as Thomas-Fermi kinetic energy density. Because $D_0(\mathbf{r})$ is brought forward the ELF as origin, what the ELF shows is an affiliate localization.

Notice that the surfaces of LOL are much more complex than electron density, so it is very difficult to locate all CPs.

The nanoclusters of (a) $\text{Si}_5\text{O}_{10}\text{-Ge}_5\text{O}_{10}$, (b) $\text{Li}_2[\text{Si}_5\text{O}_{10}\text{-Ge}_5\text{O}_{10}]$, (c) $\text{H}_2[\text{Si}_5\text{O}_{10}\text{-Ge}_5\text{O}_{10}]$ and (d) $\text{Li}_2\text{H}_4[\text{Si}_5\text{O}_{10}\text{-Ge}_5\text{O}_{10}]$ can be defined by LOL graphs owing to exploring their delocalization/localization characterizations of electrons and chemical bonds (Figure 6a-d). Covalent zones have high LOL value, the electron depletion zones between valence shell and inner shell are indicated by the blue circles around nuclei (Figure 6a-d).



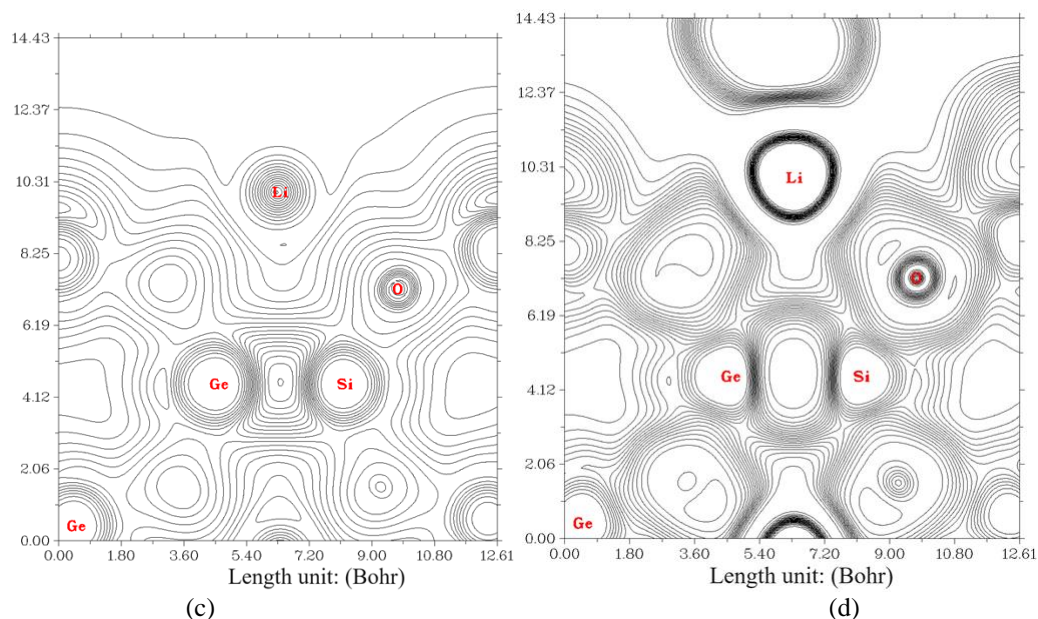
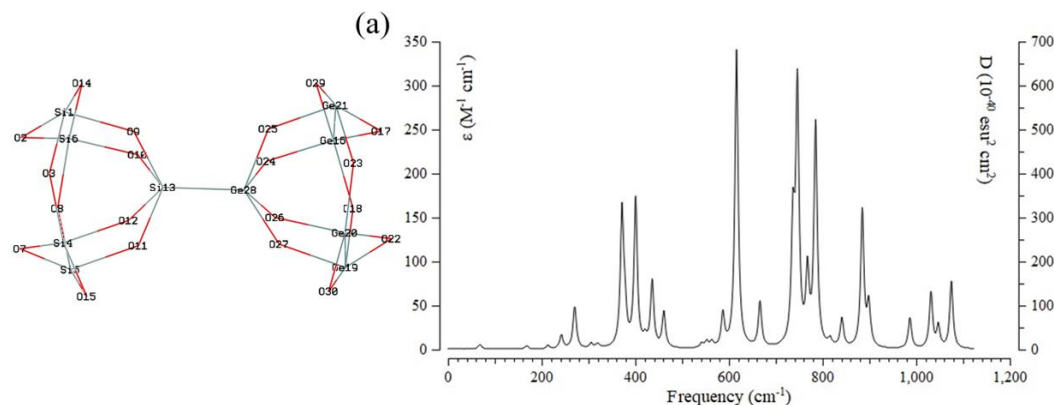


Figure 6. The graphs of LOL for (a) $\text{Si}_5\text{O}_{10}\text{-Ge}_5\text{O}_{10}$, (b) $\text{H}_2[\text{Si}_5\text{O}_{10}\text{-Ge}_5\text{O}_{10}]$, (c) $\text{Li}_2[\text{Si}_5\text{O}_{10}\text{-Ge}_5\text{O}_{10}]$ and (d) $\text{Li}_2\text{H}_4[\text{Si}_5\text{O}_{10}\text{-Ge}_5\text{O}_{10}]$

An isosurface map for $\text{Si}_5\text{O}_{10}\text{-Ge}_5\text{O}_{10}$ cluster (Figure 6a) means that electron delocalization in $\text{Si}_5\text{O}_{10}\text{-Ge}_5\text{O}_{10}$ cluster toward $\text{H}_2[\text{Si}_5\text{O}_{10}\text{-Ge}_5\text{O}_{10}]$ (Figure 6b) is easier than Si_5O_{10} or Ge_5O_{10} . However, a vaster jointed area engaged by an isosurface map for $\text{Si}_5\text{O}_{10}\text{-Ge}_5\text{O}_{10}$ cluster (Figure 6c) means that electron delocalization in $\text{Li}_2[\text{Si}_5\text{O}_{10}\text{-Ge}_5\text{O}_{10}]$ cluster toward $\text{Li}_2\text{H}_4[\text{Si}_5\text{O}_{10}\text{-Ge}_5\text{O}_{10}]$ (Figure 6d) is easier than $\text{Si}_5\text{O}_{10}\text{-Ge}_5\text{O}_{10}$ and a narrower connected area occupied by an isosurface map means that electron delocalization is relatively difficult. In fact, the counter map of LOL can confirm that $\text{Li}_2[\text{Si}_5\text{O}_{10}\text{-Ge}_5\text{O}_{10}]$ nanocluster can increase the efficiency during hydrogen adsorption towards formation of $\text{Li}_2\text{H}_4[\text{Si}_5\text{O}_{10}\text{-Ge}_5\text{O}_{10}]$ as designing novel materials for energy storage in the lithium-ion batteries.

3.6. Insight of infrared spectroscopy & thermochemistry

Infrared spectroscopy (IR) has been performed for hydrogen grabbing by $\text{Si}_5\text{O}_{10}\text{-Ge}_5\text{O}_{10}$ and $\text{Li}_2[\text{Si}_5\text{O}_{10}\text{-Ge}_5\text{O}_{10}]$ nanoclusters. Therefore, it has been simulated the several clusters containing $\text{Si}_5\text{O}_{10}\text{-Ge}_5\text{O}_{10}$ (Figure 7a), $\text{H}_2[\text{Si}_5\text{O}_{10}\text{-Ge}_5\text{O}_{10}]$ (Figure 7b), $\text{Li}_2[\text{Si}_5\text{O}_{10}\text{-Ge}_5\text{O}_{10}]$ (Figure 7c) and $\text{Li}_2\text{H}_4[\text{Si}_5\text{O}_{10}\text{-Ge}_5\text{O}_{10}]$ (Figure 7d).



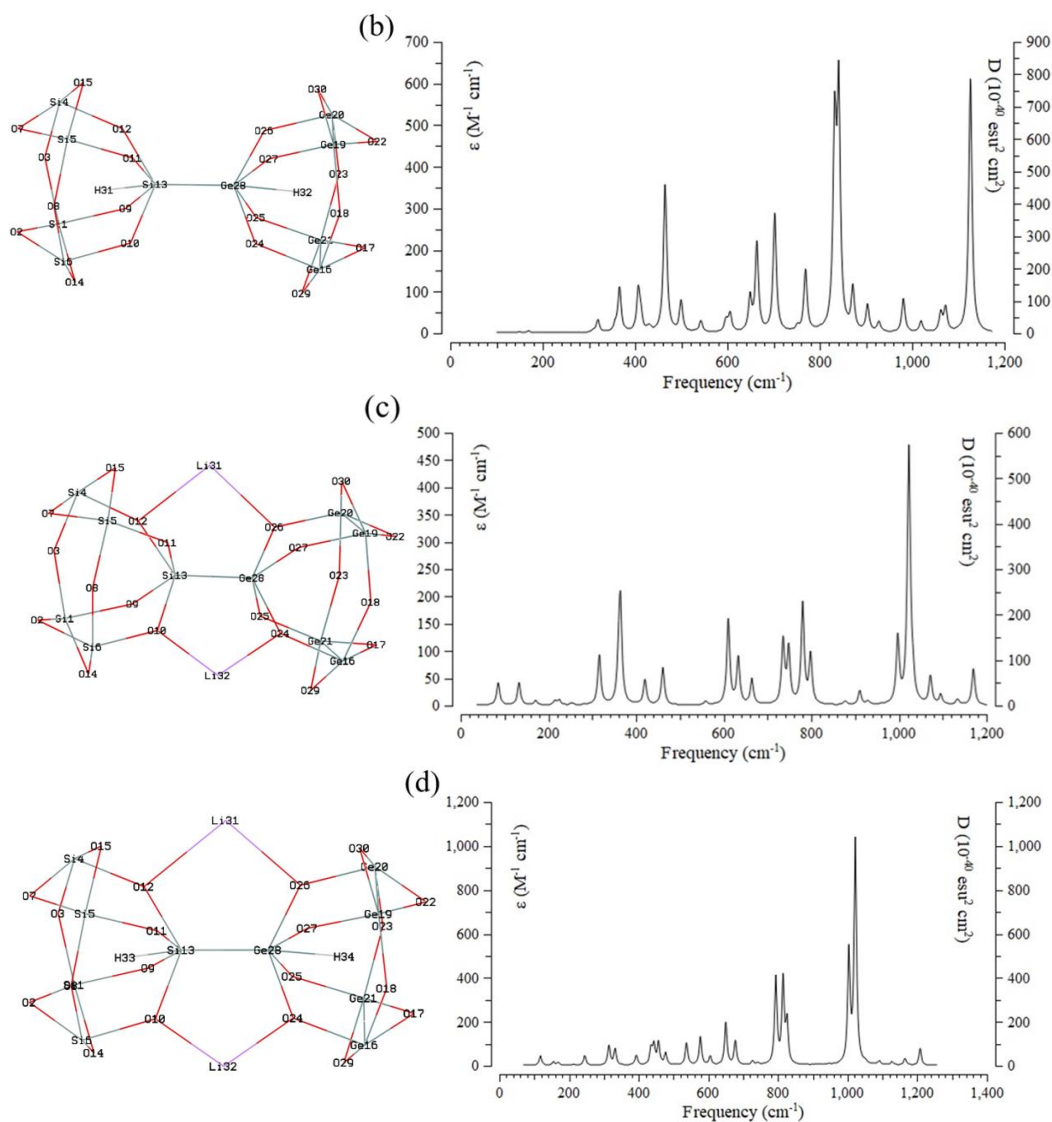


Figure 7. The Frequency (cm^{-1}) changes through the IR spectra for (a) $\text{Si}_5\text{O}_{10}\text{-Ge}_5\text{O}_{10}$, (b) $\text{H}_2[\text{Si}_5\text{O}_{10}\text{-Ge}_5\text{O}_{10}]$, (c) $\text{Li}_2[\text{Si}_5\text{O}_{10}\text{-Ge}_5\text{O}_{10}]$ and (d) $\text{Li}_2\text{H}_4[\text{Si}_5\text{O}_{10}\text{-Ge}_5\text{O}_{10}]$ complexes

The frequency values through the IR curves between $200\text{--}1100\text{cm}^{-1}$ have been achieved for $\text{Si}_5\text{O}_{10}\text{-Ge}_5\text{O}_{10}$ with several sharp peaks around 371.52 , 400.69 , 616.11 , 736.73 , 746.09 , 784.99 and 884.75 cm^{-1} (Figure 7a). Figure 7b has shown the frequency range between $300\text{--}1200\text{ cm}^{-1}$ for $\text{H}_2[\text{Si}_5\text{O}_{10}\text{-Ge}_5\text{O}_{10}]$ with sharp peaks around 464.86 , 663.71 , 702.49 , 832.17 , 841.00 and 1126.17 cm^{-1} . Figure 7c has indicated the fluctuation of frequency between $200\text{--}1200\text{ cm}^{-1}$ for $\text{Li}_2[\text{Si}_5\text{O}_{10}\text{-Ge}_5\text{O}_{10}]$ with sharp peaks around 364.39 , 610.61 , 780.37 and 1022.67 cm^{-1} . The graph of Figure 7d has been observed in the frequency range between $200\text{--}1200\text{ cm}^{-1}$ for $\text{Li}_2\text{H}_4[\text{Si}_5\text{O}_{10}\text{-Ge}_5\text{O}_{10}]$ with several sharp peaks around 793.72 , 814.41 , 1003.50 and 1021.96 cm^{-1} . Hydrogen capture with $\text{Si}_5\text{O}_{10}\text{-Ge}_5\text{O}_{10}$ and $\text{Li}_2[\text{Si}_5\text{O}_{10}\text{-Ge}_5\text{O}_{10}]$ nanoclusters has described that the frame of the overcoming cluster is related to $\text{Li}_2[\text{Si}_5\text{O}_{10}\text{-Ge}_5\text{O}_{10}]$ in the high amounts of frequency.

Table 4. The thermodynamic characters of (a) $\text{Si}_5\text{O}_{10}\text{-Ge}_5\text{O}_{10}$, (b) $\text{H}_2[\text{Si}_5\text{O}_{10}\text{-Ge}_5\text{O}_{10}]$, (c) $\text{Li}_2[\text{Si}_5\text{O}_{10}\text{-Ge}_5\text{O}_{10}]$ and (d) $\text{Li}_2\text{H}_4[\text{Si}_5\text{O}_{10}\text{-Ge}_5\text{O}_{10}]$ nanoclusters using CAM-B3LYP-D3/6-311+G (d,p) calculation

Compound	Dipole moment (Debye)	$\Delta E_{\text{ads}}^{\circ} \times 10^{-3}$ (kcal/mol)	$\Delta H_{\text{ads}}^{\circ} \times 10^{-3}$ (kcal/mol)	$\Delta G_{\text{ads}}^{\circ} \times 10^{-3}$ (kcal/mol)	$E_{\text{H-b}} \times 10^{-3}$ (kcal/mol)
Si_5O_{10}	0.44	-1379.64	-1379.64	-1379.64	
$\text{HSi}_5\text{O}_{10}$	0.73	-1379.93	-1379.93	-1379.96	-0.29
Ge_5O_{10}	0.80	-6981.16	-6981.16	-6981.20	
$\text{HGe}_5\text{O}_{10}$	0.95	-6981.444	-6981.44	-6981.47	-0.28
$\text{Si}_5\text{O}_{10}\text{-Ge}_5\text{O}_{10}$	1.27	-8360.86	-8360.86	-8360.89	
$\text{H}_2[\text{Si}_5\text{O}_{10}\text{-Ge}_5\text{O}_{10}]$	1.54	-8361.37	-8361.37	-8361.39	-0.51
$\text{Li}_2[\text{Si}_5\text{O}_{10}\text{-Ge}_5\text{O}_{10}]$	1.95	-9176.64	-9176.64	-9176.67	
$\text{Li}_2\text{H}_4[\text{Si}_5\text{O}_{10}\text{-Ge}_5\text{O}_{10}]$	2.48	-9178.09	-9178.09	-9178.11	-1.45

Table 4 through the thermodynamic specifications concluded that $\text{Li}_2[\text{Si}_5\text{O}_{10}\text{-Ge}_5\text{O}_{10}]$ nanocluster due might be more efficient structure for hydrogen trapping.

Thermodynamic parameters of hydrogen adsorption on $\text{Si}_5\text{O}_{10}\text{-Ge}_5\text{O}_{10}$ and $\text{Li}_2[\text{Si}_5\text{O}_{10}\text{-Ge}_5\text{O}_{10}]$ nanoclusters have been assigned through a given number of hydrogen donor sites, the stabilities of linkage of two complexes of Si_5O_{10} , Ge_5O_{10} and formation of $\text{Si}_5\text{O}_{10}\text{-Ge}_5\text{O}_{10}$ nanocluster can be considered as: $\text{Li}_2\text{H}_4[\text{Si}_5\text{O}_{10}\text{-Ge}_5\text{O}_{10}] > \text{H}_2[\text{Si}_5\text{O}_{10}\text{-Ge}_5\text{O}_{10}] > \text{HGe}_5\text{O}_{10} > \text{HSi}_5\text{O}_{10}$ complexes (Table 4).

The changes of Gibbs free energy versus dipole moment could detect the maximum efficiency of $\text{Si}_5\text{O}_{10}\text{-Ge}_5\text{O}_{10}$ for hydrogen adsorption through $\Delta G_{\text{ads}}^{\circ}$ which is related to linkage between hydrogen atoms with silicon and germanium in $\text{Si}_5\text{O}_{10}\text{-Ge}_5\text{O}_{10}$, $\text{Li}_2[\text{Si}_5\text{O}_{10}\text{-Ge}_5\text{O}_{10}]$ and formation of hydrated nanoclusters of $\text{H}_2[\text{Si}_5\text{O}_{10}\text{-Ge}_5\text{O}_{10}]$ and $\text{Li}_2\text{H}_4[\text{Si}_5\text{O}_{10}\text{-Ge}_5\text{O}_{10}]$ (Table 4).

The adsorption process of hydrogen atoms on Si_5O_{10} , Ge_5O_{10} , $\text{Si}_5\text{O}_{10}\text{-Ge}_5\text{O}_{10}$ and $\text{Li}_2[\text{Si}_5\text{O}_{10}\text{-Ge}_5\text{O}_{10}]$ nanoclusters is affirmed by the $\Delta G_{\text{ads}}^{\circ}$ quantities:

$$\Delta G_{\text{ads}(1)}^{\circ} = \Delta G_{\text{H}_2[\text{Si}_5\text{O}_{10}\text{-Ge}_5\text{O}_{10}]}^{\circ} - (\Delta G_{\text{Si}_5\text{O}_{10}}^{\circ} + \Delta G_{\text{HSi}_5\text{O}_{10}}^{\circ} + \Delta G_{\text{Ge}_5\text{O}_{10}}^{\circ} + \Delta G_{\text{HGe}_5\text{O}_{10}}^{\circ}) \quad (16)$$

$$\Delta G_{\text{ads}(2)}^{\circ} = \Delta G_{\text{Li}_2\text{H}_4[\text{Si}_5\text{O}_{10}\text{-Ge}_5\text{O}_{10}]}^{\circ} - (\Delta G_{\text{Li}_2[\text{Si}_5\text{O}_{10}\text{-Ge}_5\text{O}_{10}]}^{\circ} + \Delta G_{\text{Si}_5\text{O}_{10}\text{-Ge}_5\text{O}_{10}}^{\circ}) \quad (17)$$

Table 3 has shown the key role of interaction between the adsorbate of hydrogen atoms as the electron donors and the adsorbent of Si_5O_{10} , Ge_5O_{10} , $\text{Si}_5\text{O}_{10}\text{-Ge}_5\text{O}_{10}$ and $\text{Li}_2[\text{Si}_5\text{O}_{10}\text{-Ge}_5\text{O}_{10}]$ nanoclusters as the electron acceptors. Therefore, combination of Si_5O_{10} and Ge_5O_{10} and producing $\text{Si}_5\text{O}_{10}\text{-Ge}_5\text{O}_{10}$ nanocluster can promise enhancing hydrogen storage in the transistors through formation of the hydrated cluster of $\text{H}_2[\text{Si}_5\text{O}_{10}\text{-Ge}_5\text{O}_{10}]$. Moreover, hydrogen bond (H-bond) accepting sites by $\text{Li}_2[\text{Si}_5\text{O}_{10}\text{-Ge}_5\text{O}_{10}]$ can alleviate parasitic hydrogen evolution in aqueous electrolytes in lithium-ion batteries. The introduced nanocluster of $\text{Li}_2[\text{Si}_5\text{O}_{10}\text{-Ge}_5\text{O}_{10}]$ containing both an H-bond acceptor and donor effectively confines water molecules in a double-site anchoring configuration with strengthened H-bonding interactions and interrupts the original H-bonding among water molecules.

4. Conclusion

In summary, H-grabbing on the nanoclusters of Si_5O_{10} , Ge_5O_{10} and $\text{Si}_5\text{O}_{10}\text{-Ge}_5\text{O}_{10}$ was investigated by first-principle calculations. The alterations of charge density illustrated a remarkable charge transfer towards Si_5O_{10} , Ge_5O_{10} and $\text{Si}_5\text{O}_{10}\text{-Ge}_5\text{O}_{10}$ which might play the electron acceptor roles while H-atoms act as the stronger electron donor through adsorption on the Si_5O_{10} , Ge_5O_{10} and $\text{Si}_5\text{O}_{10}\text{-Ge}_5\text{O}_{10}$. The fluctuation in charge density values demonstrates that the electronic densities were mainly located in the boundary of adsorbate/adsorbent atoms during the adsorption status. As a matter of fact, Si_5O_{10} , Ge_5O_{10} , $\text{Si}_5\text{O}_{10}\text{-Ge}_5\text{O}_{10}$ and $\text{Li}_2[\text{Si}_5\text{O}_{10}\text{-Ge}_5\text{O}_{10}]$ have greater interaction energy from Van der Waals' forces with H-atoms that can cause them to be much more resistant. Besides, thermodynamic parameters describing H-grabbing on the nano-carbides of Si_5O_{10} , Ge_5O_{10} and $\text{Si}_5\text{O}_{10}\text{-Ge}_5\text{O}_{10}$ have been investigated including internal process of the adsorbent-adsorbate system. Combination of Si_5O_{10} and Ge_5O_{10} and producing $\text{Si}_5\text{O}_{10}\text{-Ge}_5\text{O}_{10}$ nanocluster can promise enhancing hydrogen storage in the transistors through formation of the hydrated clusters of $\text{H}_2[\text{Si}_5\text{O}_{10}\text{-Ge}_5\text{O}_{10}]$. Moreover, hydrogen bond (H-bond) accepting sites by $\text{Li}_2[\text{Si}_5\text{O}_{10}\text{-Ge}_5\text{O}_{10}]$ can alleviate parasitic hydrogen evolution in aqueous electrolytes in lithium-ion batteries. Thermodynamic parameters have constructed a detailed molecular model for atom-atom interactions and a distribution of point charges which can be utilized to reproduce the polarity of the solid material and the adsorbing molecules. Today, it is crucial to distinguish the potential of hydrogen technologies and bring up all perspectives of their performance, from technological progresses to economic and social effects. The authors intend to pursue research on sustainability and clean energy subjects towards finding new solutions for reducing the global dependency on fossil fuels.

Acknowledgements

In successfully completing this paper and its research, the authors are grateful to Kastamonu University.

References

- Arrigoni, M., Madsen, G.K. (2019). Comparing the performance of LDA and GGA functionals in predicting the lattice thermal conductivity of III-V semiconductor materials in the zincblende structure: The cases of AlAs and BaS. *Computational Materials Science*, 156, 354-360.
- Bakhshi, K., Mollaamin, F. & Monajjemi, A.M. (2011). Exchange and correlation effect of hydrogen chemisorption on nano V (100) surface: A DFT study by generalized gradient approximation (GGA). *Journal of Computational and Theoretical Nanoscience*, 8(4), 763-768. <https://doi.org/10.1166/jctn.2011.1750>
- Baughman, R.H., Zakhidov, A.A. & De Heer, W.A. (2002). Carbon nanotubes-the route toward applications. *Science*, 297(5582), 787-792. <https://doi.org/10.1126/science.1060928>
- Becke, A.D. (1993). Density-functional thermochemistry. III. The role of exact exchange. *The Journal of Chemical Physics*, 98(7), 5648-5652. <https://doi.org/10.1063/1.464913>
- Blöchl, P.E. (1994). Projector augmented-wave method. *Physical Review B*, 50(24), 17953.
- Castro Neto, A.H., Guinea, F., Peres, N.M., Novoselov, K.S. & Geim, A.K. (2009). The electronic properties of graphene. *Reviews of Modern Physics*, 81(1), 109-162.
- Chettri, B., Patra, P.K., Srivastava, S., Lalhriatualala, Z.L. & Rai, D.P. (2019). Electronic properties of hydrogenated hexagonal boron nitride (h-BN): DFT study. *Senhri Journal of Multidisciplinary Studies*, 4, 72-79. <https://doi.org/10.36110/sjms.2019.04.02.008>

- Cramer, C.J. (2013). *Essentials of Computational Chemistry: Theories and Models*. John Wiley & Sons. Retrieved 2021-06-24.
- Das, V., Padmanaban, S., Venkitesamy, K., Selvamuthukumar, R., Blaabjerg, F. & Siano, P. (2017). Recent advances and challenges of fuel cell based power system architectures and control-A review. *Renewable and Sustainable Energy Reviews*, 73, 10-18. <https://doi.org/10.1016/j.rser.2017.01.148>
- Dennington, R.D.I.I., Keith, T.A. & Millam, J.M. (2016). GaussView, version 6.0.16. Semichem Inc Shawnee Mission KS.
- Fei, R., Faghaninia, A., Soklaski, R., Yan, J.A., Lo, C. & Yang, L. (2014). Enhanced thermoelectric efficiency via orthogonal electrical and thermal conductances in phosphorene. *Nano Letters*, 14(11), 6393-6399.
- Feng, X., Sun, L., Wang, W., Zhao, Y. & Shi, J.W. (2023). Construction of CdS@ZnO core-shell nanorod arrays by atomic layer deposition for efficient photoelectrochemical H₂ evolution. *Separation and Purification Technology*, 324, 124520. <https://doi.org/10.1016/j.seppur.2023.124520>
- Frisch, M.J., Trucks, G.W., Schlegel, H.B., Scuseria, G.E. & Robb, M.A. (2016). Gaussian 16. Revision C.01.
- Geim, A.K. (2009). Graphene: Status and prospects. *Science*, 324(5934), 1530-1534.
- Grimme, S., Antony, J., Ehrlich, S. & Krieg, H. (2010). A consistent and accurate ab initio parametrization of density functional dispersion correction (DFT-D) for the 94 elements H-Pu. *The Journal of Chemical Physics*, 132(15). <https://doi.org/10.1063/1.3382344>
- Hammad, A., Dincer, I. (2018). Analysis and assessment of an advanced hydrogen liquefaction system. *International Journal of Hydrogen Energy*, 43(2), 1139-1151. <https://doi.org/10.1016/j.ijhydene.2017.10.158>
- Henkelman, G., Arnaldsson, A. & Jónsson, H. (2006). A fast and robust algorithm for Bader decomposition of charge density. *Computational Materials Science*, 36(3), 354-360.
- Hohenberg, P., Kohn, W. (1964). Inhomogeneous electron gas. *Physical Review*, 136(3B), B864.
- Jacobsen, H. (2008). Localized-orbital locator (LOL) profiles of chemical bonding. *Canadian Journal of Chemistry*, 86(7), 695-702. <https://doi.org/10.1139/v08-052>
- Javan, M.B. (2016). Electronic and magnetic properties of monolayer SiC sheet doped with 3d-transition metals. *Journal of Magnetism and Magnetic Materials*, 401, 656-661.
- Kim, K., Jordan, K.D. (1994). Comparison of density functional and MP2 calculations on the water monomer and dimer. *The Journal of Physical Chemistry*, 98(40), 10089-<https://doi.org/10.1021/j100091a024>
- Kohn, W., Sham, L.J. (1965). Self-consistent equations including exchange and correlation effects. *Physical Review*, 140(4A), A1133.
- Lee, C., Yang, W. & Parr, R.G. (1988). Development of the Colle-Salvetti correlation-energy formula into a functional of the electron density. *Physical review B*, 37(2), 785.
- Lobo, R., Ribeiro, J. & Inok, F. (2021). Hydrogen uptake and release in carbon nanotube electrocatalysts. *Nanomaterials*, 11(4), 975. <https://doi.org/10.3390/nano11040975>
- Low, T., Rodin, A.S., Carvalho, A., Jiang, Y., Wang, H., Xia, F. & Castro Neto, A. H. (2014). Tunable optical properties of multilayer black phosphorus thin films. *Physical Review B*, 90(7), 075434.
- Luo, J., Wang, C., Wang, Z., Guo, Q., Yang, J., Zhou, R. & Zheng, G.Q. (2020). NMR and NQR studies on transition-metal arsenide superconductors LaRu₂As₂, KCa₂Fe₄As₄F₂ and A₂Cr₃As₃. *Chinese Physics B*, 29(6), 067402. <https://doi.org/10.1088/1674-1056/ab892d>
- Mak, K.F., Lee, C., Hone, J., Shan, J. & Heinz, T.F. (2010). Atomically thin MoS₂: A new direct-gap semiconductor. *Physical Review Letters*, 105(13), 136805.
- Matta, C.F., Ayers, P.W. & Cook, R. (2024). The Physics of electron localization and delocalization. In *Electron Localization-Delocalization Matrices*, 7-20. Springer International Publishing. https://doi.org/10.1007/978-3-031-51434-0_2
- Mollaamin, F. (2024). Competitive intracellular hydrogen-nanocarrier among aluminum, carbon or silicon implantation: A novel technology of eco-friendly energy storage using research

- density functional theory. *Russian Journal of Physical Chemistry B*, 18(3), 805-820. <https://doi.org/10.1134/S1990793124700131>
- Mollaamin, F., & Monajjemi, M. (2023). Molecular modelling framework of metal-organic clusters for conserving surfaces: Langmuir sorption through the TD-DFT/ONIOM approach. *Molecular Simulation*, 49(4), 365-376. <https://doi.org/10.1080/08927022.2022.2159996>
- Mollaamin, F., Monajjemi, M. (2024). Adsorption ability of Ga₅N₁₀ nanomaterial for removing metal ions contamination from drinking water by DFT. *International Journal of Quantum Chemistry*, 124(2), e27348. <https://doi.org/10.1002/qua.27348>
- Mollaamin, F., Monajjemi, M. (2024). In situ Ti-embedded SiC as chemiresistive nanosensor for safety monitoring of CO, CO₂, NO, NO₂: Molecular Modelling by conceptual density functional theory. *Russian Journal of Physical Chemistry B*, 18(1), 49-66. <https://doi.org/10.1134/S1990793124010159>
- Mollaamin, F., Monajjemi, M. (2024). Nanomaterials for sustainable energy in hydrogen-fuel cell: Functionalization and characterization of carbon nano-semiconductors with silicon, germanium, tin or lead through density functional theory study. *Russian Journal of Physical Chemistry B*, 18(2), 607-623. <https://doi.org/10.1134/S1990793124020271>
- Mollaamin, F., Baei, M.T., Monajjemi, M., Zhiani, R. & Honarparvar, B. (2008). A DFT study of hydrogen chemisorption on v (100) surfaces. *Russian Journal of Physical Chemistry A, Focus on Chemistry*, 82(13), 2354-2361. <https://doi.org/10.1134/S0036024408130323>
- Mollaamin, F., Shahriari, S. & Monajjemi, M. (2024). Influence of transition metals for emergence of energy storage in fuel cells through hydrogen adsorption on the MgAl surface. *Russian Journal of Physical Chemistry B*, 18(2), 398-418. <https://doi.org/10.1134/S199079312402026X>
- Monajjemi, M., Mollaamin, F. (2024). Development of solid-state lithium-ion batteries (LIBs) to increase ionic conductivity through interactions between solid electrolytes and anode and cathode electrodes. *Energies*, 17(18), 4530. <https://doi.org/10.3390/en17184530>
- Monajjemi, M., Baei, M.T. & Mollaamin, F. (2008). Quantum mechanic study of hydrogen chemisorptions on nanocluster vanadium surface. *Russian journal of inorganic chemistry*, 53, 1430-1437. <https://doi.org/10.1134/S0036023608090143>
- Nazeer, W., Farooq, A., Younas, M., Munir, M. & Kang, S.M. (2018). On molecular descriptors of carbon nanocones. *Biomolecules*, 8(3), 92. <https://doi.org/10.3390/biom8030092>
- Novoselov, K.S., Geim, A.K., Morozov, S.V., Jiang, D.E., Zhang, Y., Dubonos, S.V. & Firsov, A.A. (2004). Electric field effect in atomically thin carbon films. *Science*, 306(5696), 666-669.
- O'boyle, N.M., Tenderholt, A.L. & Langner, K.M. (2008). Cclic: A library for package-independent computational chemistry algorithms. *Journal of Computational Chemistry*, 29(5), 839-845.
- Olabi, A.G., Sayed, E.T. (2023). Developments in hydrogen fuel cells. *Energies*, 16(5), 2431. <https://doi.org/10.3390/en16052431>
- Perdew, J.P., Burke, K. & Ernzerhof, M. (1996). Generalized gradient approximation made simple. *Physical Review Letters*, 77(18), 3865.
- Piñero, J.J., Ramírez, P.J., Bromley, S.T., Illas, F., Viñes, F. & Rodriguez, J.A. (2018). Diversity of adsorbed hydrogen on the TiC (001) surface at high coverages. *The Journal of Physical Chemistry C*, 122(49), 28013-28020. <https://doi.org/10.1021/acs.jpcc.8b07340>
- Qyyum, M.A., Chaniago, Y.D., Ali, W., Saulat, H. & Lee, M. (2020). Membrane-assisted removal of hydrogen and nitrogen from synthetic natural gas for energy-efficient liquefaction. *Energies*, 13(19), 5023. <https://doi.org/10.3390/en13195023>
- Radisavljevic, B., Radenovic, A., Brivio, J., Giacometti, V. & Kis, A. (2011). Single-layer MoS₂ transistors. *Nature Nanotechnology*, 6(3), 147-150.
- Ramasubramaniam, A., Muniz, A.R. (2014). Ab initio studies of thermodynamic and electronic properties of phosphorene nanoribbons. *Physical Review B*, 90(8), 085424.

- Reza, M.S., Mannan, M., Wali, S.B., Hannan, M.A., Jern, K.P., Rahman, S.A. & Mahlia, T.I. (2021). Energy storage integration towards achieving grid decarbonization: A bibliometric analysis and future directions. *Journal of Energy Storage*, 41, 102855. <https://doi.org/10.1016/j.est.2021.102855>
- Rivard, E., Trudeau, M. & Zaghbi, K. (2019). Hydrogen storage for mobility: A review. *Materials*, 12(12), 1973. <https://doi.org/10.3390/ma12121973>
- Rodin, A.S., Carvalho, A. & Castro Neto, A.H. (2014). Strain-induced gap modification in black phosphorus. *Physical Review Letters*, 112(17), 176801.
- Rong, Y., Cao, Y., Guo, N., Li, Y., Jia, W. & Jia, D. (2016). A simple method to synthesize V₂O₅ nanostructures with controllable morphology for high performance Li-ion batteries. *Electrochimica Acta*, 222, 1691-1699. <https://doi.org/10.1016/j.electacta.2016.11.160>
- Savin, A., Jepsen, O., Flad, J., Andersen, O.K., Preuss, H. & von Schnering, H.G. (1992). Electron localization in solid-state structures of the elements: The diamond structure. *Angewandte Chemie International Edition in English*, 31(2), 187-188. <https://doi.org/10.1002/anie.199201871>
- Schmider, H.L., Becke, A.D. (2000). Chemical content of the kinetic energy density. *Journal of Molecular Structure: THEOCHEM*, 527(1-3), 51-61. [https://doi.org/10.1016/S0166-1280\(00\)00477-2](https://doi.org/10.1016/S0166-1280(00)00477-2)
- Sciotto, R., Ruiz Alvarado, I.A. & Schmidt, W.G. (2024). Substrate doping and defect influence on P-Rich InP (001): H surface properties. *Surfaces*, 7(1), 79-87. <https://doi.org/10.3390/surfaces7010006>
- Sohail, U., Ullah, F., Binti Zainal Arfan, N.H., Abdul Hamid, M.H.S., Mahmood, T., Sheikh, N. S. & Ayub, K. (2023). Transition metal sensing with nitrogenated holey graphene: A first-principles investigation. *Molecules*, 28(10), 4060. <https://doi.org/10.3390/molecules28104060>
- Stephens, P.J., Devlin, F.J., Chabalowski, C.F. & Frisch, M.J. (1994). Ab initio calculation of vibrational absorption and circular dichroism spectra using density functional force fields. *The Journal of Physical Chemistry*, 98(45), 11623-11627. <https://doi.org/10.1021/j100096a001>
- Taha, H.O., El Mahdy, A.M., El Shemy, F.E.S. & Hassan, M.M. (2023). Hydrogen storage in SiC, GeC and SnC nanocones functionalized with nickel, Density Functional Theory-Study. *International Journal of Quantum Chemistry*, 123(3), e27023. <https://doi.org/10.1002/qua.27023>
- Thupsuri, S., Tabtimsai, C., Ruangpornvisuti, V. & Wannoo, B. (2021). A study of the transition metal doped boron nitride nanosheets as promising candidates for hydrogen and formaldehyde adsorptions. *Physica E: Low-dimensional Systems and Nanostructures*, 134, 114859. <https://doi.org/10.1016/j.physe.2021.114859>
- Tian, L., Feiwu, C. (2011). Meaning and functional form of the electron localization function. *Acta Physico-Chimica Sinica*, 27(12), 2786-2792. <https://doi.org/10.3866/PKU.WHXB20112786>
- Trontelj, Z., Pirnat, J., Jazbinšek, V., Lužnik, J., Srčič, S., Lavrič, Z. & Seliger, J. (2020). Nuclear quadrupole resonance (NQR)-a useful spectroscopic tool in pharmacy for the study of polymorphism. *Crystals*, 10(6), 450. <https://doi.org/10.3390/cryst10060450>
- Tsirelson, V.G., Stash, A. (2002). Analyzing experimental electron density with the localized-orbital locator. *Acta Crystallographica Section B: Structural Science*, 58(5), 780-785. <https://doi.org/10.1107/S0108768102012338>
- Vosko, S.H., Wilk, L. & Nusair, M. (1980). Accurate spin-dependent electron liquid correlation energies for local spin density calculations: A critical analysis. *Canadian Journal of physics*, 58(8), 1200-1211. <https://doi.org/10.1139/p80-159>
- Wu, Y., Zhou, L., Du, X. & Yang, Y. (2015). Near-field radiative heat transfer between two SiC plates with/without coated metal films. *Journal of Nanoscience and Nanotechnology*, 15(4), 3017-3024.

- Yan, Z., Bai, Y. & Sun, L. (2019). Adsorption of thiophene and SO_x molecules on Cr-doped and Ti-doped graphene nanosheets: A DFT study. *Materials Research Express*, 6(12), 125067. <https://doi.org/10.1088/2053-1591/ab599d>
- Yanai, T., Tew, D.P. & Handy, N.C. (2004). A new hybrid exchange-correlation functional using the Coulomb-attenuating method (CAM-B3LYP). *Chemical Physics Letters*, 393(1-3), 51-57. <https://doi.org/10.1016/j.cplett.2004.06.011>
- Yang, C.M., Kanoh, H., Kaneko, K., Yudasaka, M. & Iijima, S. (2002). Adsorption behaviors of HiPco single-walled carbon nanotube aggregates for alcohol vapors. *The Journal of Physical Chemistry B*, 106(35), 8994-8999.
- Yang, F.H., Lachawiec, A.J. & Yang, R.T. (2006). Adsorption of spillover hydrogen atoms on single-wall carbon nanotubes. *The Journal of Physical Chemistry B*, 110(12), 6236-6244. <https://doi.org/10.1021/jp056461u>
- Yodsin, N., Sakagami, H., Udagawa, T., Ishimoto, T., Jungsuttiwong, S. & Tachikawa, M. (2021). Metal-doped carbon nanocones as highly efficient catalysts for hydrogen storage: Nuclear quantum effect on hydrogen spillover mechanism. *Molecular Catalysis*, 504, 111486. <https://doi.org/10.1016/j.mcat.2021.111486>
- Young, H.D., Freedman, R.A. & Ford, A.L. (2008). *Sears and Zemansky's University Physics*, 1. Pearson education.
- Yu, X., Zhang, X., Wang, H., Wang, Z. & Feng, G. (2017). High-coverage H₂ adsorption on the reconstructed Cu₂O (111) surface. *The Journal of Physical Chemistry C*, 121(40), 22081-22091. <https://doi.org/10.1021/acs.jpcc.7b06361>
- Zavoisky, E. (1945). Spin-magnetic resonance in paramagnetics. *Journal of Physics USSR*, 9, 211-245.
- Zhao, J., Li, Z., Cole, M.T., Wang, A., Guo, X., Liu, X. & Dai, Q. (2021). Nanocone-shaped carbon nanotubes field-emitter array fabricated by laser ablation. *Nanomaterials*, 11(12), 3244. <https://doi.org/10.3390/nano11123244>
- Ziesche, P., Kurth, S. & Perdew, J.P. (1998). Density functionals from LDA to GGA. *Computational Materials Science*, 11(2), 122-127.